Article

Prospects of Using Small Scale Testing to Examine Different Deformation Mechanisms in Nanoscale Single Crystals—A Case Study in Mg

Daniel Kiener [1],*, Jiwon Jeong [2,3], Markus Alfreider [1], Ruth Konetschnik [1] and Sang Ho Oh [2,4,*]

[1] Department Materials Science, Chair of Materials Physics, Montanuniversität Leoben, Roseggerstrasse 12, 8700 Leoben, Austria; markus.alfreider@unileoben.ac.at (M.A.); r.konetschnik@gmail.com (R.K.)
[2] Department of Materials Science and Engineering, Pohang University of Science and Technology (POSTECH), Pohang 37673, Korea; j.jeong@mpie.de
[3] Department of Structure and Nano-/Micromechanics of Materials, Max-Planck Institut für Eisenforschung GmbH, 40237 Düsseldorf, Germany
[4] Department of Energy Science, Sungkyunkwan University (SKKU), Suwon 16419, Korea
*   Correspondence: daniel.kiener@unileoben.ac.at (D.K.); sanghooh@skku.edu (S.H.O.)

Abstract: The advent of miniaturised testing techniques led to excessive studies on size effects in materials. Concomitantly, these techniques also offer the capability to thoroughly examine deformation mechanisms operative in small volumes, in particular when performed in-situ in electron microscopes. This opens the feasibility of a comprehensive assessment of plasticity by spatially arranging samples specifically with respect to the crystal unit cell of interest. In the present manuscript, we will showcase this less commonly utilised aspect of small-scale testing on the case of the hexagonal metal Mg, where, besides dislocation slip on different slip planes, twinning also exists as a possible deformation mechanism. While it is close to impossible to examine individual deformation mechanisms in macroscale tests, where local multiaxial stress states in polycrystalline structures will always favour multiple mechanisms of plasticity, we demonstrate that miniaturised uniaxial experiments conducted in-situ in the scanning electron microscope are ideally suited for a detailed assessment of specific processes.

Keywords: dislocation plasticity; twinning; miniaturised testing; in situ electron microscopy; magnesium

1. Introduction

Small scale experiments have provided numerous insights regarding the mechanical properties of confined volumes. This is largely owed to the fact that by testing small volumes, individual constituents of the microstructure can be examined. Since the first report on the intriguing mechanical properties of micron sized metallic objects [1], understanding related size effects was a prime driver of research in the micromechanics community [2,3]. Sparked by this initial discovery, the activities and interests continuously grew and spread into many different routes of research, which cannot be covered within the scope of this article. One of the first subsequent questions that received considerable interest regarded the effect of specific or multiple interfaces within a small probed volume [4–7], while another facet of experimental efforts concerned the deformation mechanisms in more complex crystal structures such as hexagonal-close packed metals (Mg [8,9] or Ti [10,11]).

The deformation of Mg is accommodated by deformation twinning (tensile twin, contraction twin) or dislocation slip (basal <a>, prismatic <a>, and pyramidal <c+a> slip). Each deformation mode has been investigated in order to understand the fundamentals of the anisotropic deformation behaviour in Mg. In the case of <a> basal slip, the deformation mechanism appears quite similar to that of face-centred cubic metals, because <a> dislocations are easily nucleated and glide on basal planes [12]. In the case of <c+a> pyramidal slip, however, the deformation behaviour is quite different compared to <a> basal slip,

because <c+a> dislocations cannot easily glide on their slip plane due to the large Burgers vector and the high Peierls stress of pyramidal planes [8,9,13–15]. In the case of the $\{10\bar{1}2\}$ tensile twin, the twinning mechanism is still not well understood and under debate because of the extremely small twinning shear compared to the other twinning modes [16,17].

Thinking beyond the significant open questions that still exist for pure magnesium, one might be interested, for example, in aspects concerning the critical resolved shear stress of certain deformation mechanisms [12,18,19] or the influence of alloying on solid solution strengthening and precipitation hardening affecting the material twinnability [20,21].

With the increasing complexity of the research in question, it becomes more and more demanding to assess the single crystal properties for a fundamental understanding rather than just examining the bulk response of a new experimental alloy. This is where the strength of small scale testing should be embraced, as it allows comprehensive testing utilising only minimal amounts of material. Thus, the intention of this manuscript is to demonstrate the feasibility to test all fundamental deformation mechanisms of magnesium utilising only a small material volume. Due to the large difference in the activation energy of each deformation mode in Mg, strongly anisotropic deformation behaviours can be investigated depending on loading axes and conditions. While this allows not only the examination of the influence of crystal orientation, but also the impact of crystal size, strain rate and deformation temperature on the resulting mechanical response, we will limit this consideration to the fundamental modes of deformation, the related extensions towards the mentioned other variables are trivial but beyond the scope of this work.

As such, in the remainder we will detail a possible testing scheme using in-situ testing in the scanning electron microscope (SEM), apply it to the defined fundamental hexagonal crystal orientations, and detail the resultant deformation features and their relation to previous works.

2. Experimental

For this study, a Magnesium single crystal of high purity (better than 99.999%) was purchased from Goodfellow Cambridge Ltd. (Huntingdon, United Kingdom) to ascertain a homogenous chemistry and avoid any influences from chemical segregation or inhomogeneities on the results. To expose the crystalline faces and directions of interest for testing in this study, thin slices were cut from the pre-oriented single crystal using a slow speed diamond wire saw and shaped to resemble the geometry of half-moon samples for transmission electron microscopy (TEM). These samples were subsequently etched in a water-free solution consisting of 5 mL HNO_3 and 95 mL ethanol to avoid unintended oxidation of Mg and remove material potentially deformed due to the previous sawing process. Subsequently, miniaturised compression and tensile samples were fabricated along the chemically thinned wedge as shown exemplarily in Figure 1 and insets therein using a focussed ion beam (FIB, Leo 1540 XB, Carl Zeiss, Oberkochen, Germany). The acceleration voltage of the Ga ion beam was 30 keV, and the ion beam currents were gradually decreased from starting 5 nA for rough milling down to 10 pA for final polishing of the specimen surfaces. All samples were placed on somewhat larger pedestals seen in the overview in Figure 1 to provide a clear measure of potential sample sink-in [22] during in-situ testing. Furthermore, micro-compression samples have typical aspect ratios between 4:1 and 3:1 to avoid potential plastic buckling [22], while micro-tensile specimens have commonly aspect ratios of 5:1 [23]. For details on these sample fabrication strategies, please refer to [24,25]. By fabricating the samples along the wedge, many of them can be placed in close proximity of a few microns, while at the same time a free line of sight is ensured in order to facilitate in-situ testing or other means of analysis.
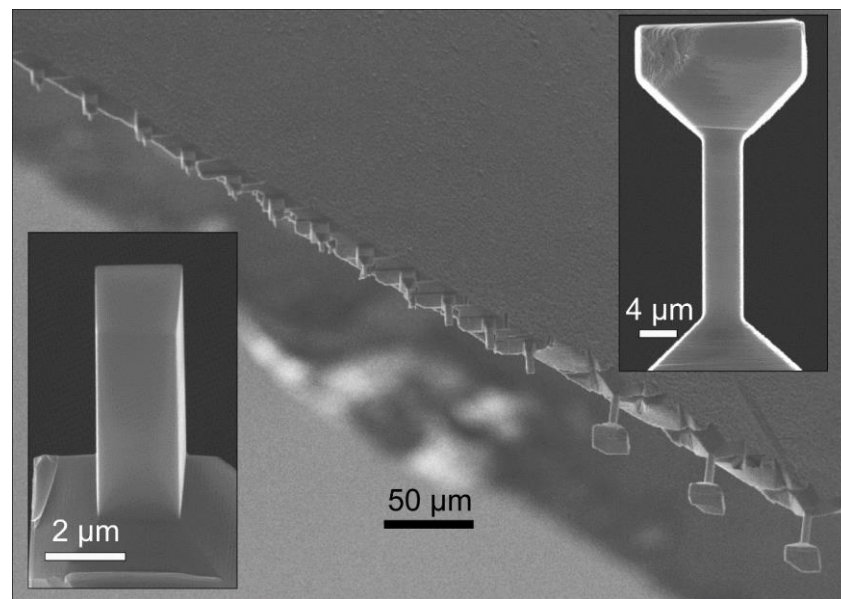
Figure 1. Low magnification SEM overview image of a series of differently sized compression and tensile samples before testing. The insets show a representative tensile and compression specimen, respectively.

Furthermore, it is essential to fabricate the samples with a well-defined orientation in a rigorous coordinate system and avoid all geometrical deficiencies. At the same time, the specimens should be transferrable between the FIB employed for specimen fabrication, the dedicated in-situ testing scanning electron microscope (SEM, DSM982, Carl Zeiss AG, Oberkochen, Germany), as well as the TEM (JEM 2100F, Jeol Ltd., Tokyo, Japan) for additional high resolution characterisation. Thus, we developed a staggered holder design as shown in Figure 2. The actual TEM-inspired sample has a flat along its circumference to ensure rotational alignment. Thus, even after repeated placement in a TEM, rotational alignment is kept [26]. This half-disk is mounted in a holder suited to fit the Bruker Hysitron Picoindenter PI-85 SEM as well as the PI-95 TEM nanoindenter with a clamping grip. As stated before, with the rotational degree of freedom fixed, the alignment during uniaxial testing is given. Finally, this whole SEM/TEM testing compatible holder can be placed in a larger mounting device that is on the one hand compatible to the Asmec UNAT 1 in-situ SEM microindenter, while on the other hand, this holder is used for the FIB processing, as it allows for controlled rotations of the mounted sample by $\pm 45°$ and $\pm 90°$, as well as tilt along the long axis by $90°$. Thus, by re-mounting the specimen at various tilts, perfect rectangular and orthogonal specimens with constant sample cross-sections can be fabricated. Moreover, utilising the $\pm 45°$ tilts allows the specimens to be rotated by $45°$ with respect to the wedge, which provides a view on two faces rather than a single one during in-situ testing, which is a particular benefit during in-situ SEM testing [4,5].
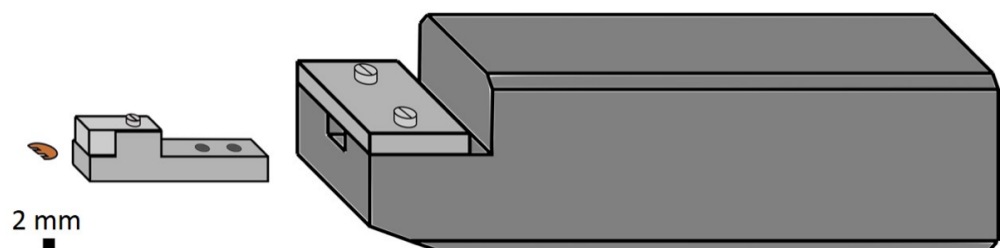

Figure 2. Specimen mounting and transfer concept. The actual sample follows a TEM specimen geometry, with adaptive holders to fit to different in situ TEM/SEM testing platforms as well as general focussed ion beam (FIB) fabrication and post testing SEM analysis.

The specimen sizes discussed here will be kept in the micrometre regime, spanning between 2 μm and 4 μm, respectively, taking into account that the emphasis of the present study is placed on bulk deformation mechanisms rather than effects specific to a nanoscale sample nature. While the strength values might thus be to some extent affected by the specimen size, the dimensions are above the typical dislocation spacing in well annealed crystals [27]. As such, we expect largely bulk deformation mechanisms to be examined [28].

The transferable sample mounting scheme proves a valuable asset also to examine the initial crystal orientation. Deviations from the planned crystallography could cause activation of unintended slip systems. So could the presence of unnoticed growth twins or occurring small angle boundaries [29]. While the crystallographic orientation of the specimen can be routinely accessed using electron backscatter diffraction (EBSD), with some effort even in a quasi in-situ manner [11], the orientation information from diffraction information in the TEM is much more sensitive, in particular with respect to low angle crystal defects that are challenging to resolve by standard EBSD. Furthermore, the effect of surface oxides or presence of initial dislocations can be easily assessed. Here, the specimens were routinely analysed using TEM, and an example for a 4-μm Mg tensile specimen is shown in Figure 3. Of course the sample is not fully electron transparent over the entire cross-section, but the whole length along both edges can be inspected for crystallographic defects, as exemplarily shown in Figure 3a,b for the bottom and head part of the sample, and the diffraction information in these regions is assessable, as shown for regions 3 and 4 in Figure 3c,d, to detail the crystallographic loading direction. In analogy, samples can be inspected post testing in the TEM.
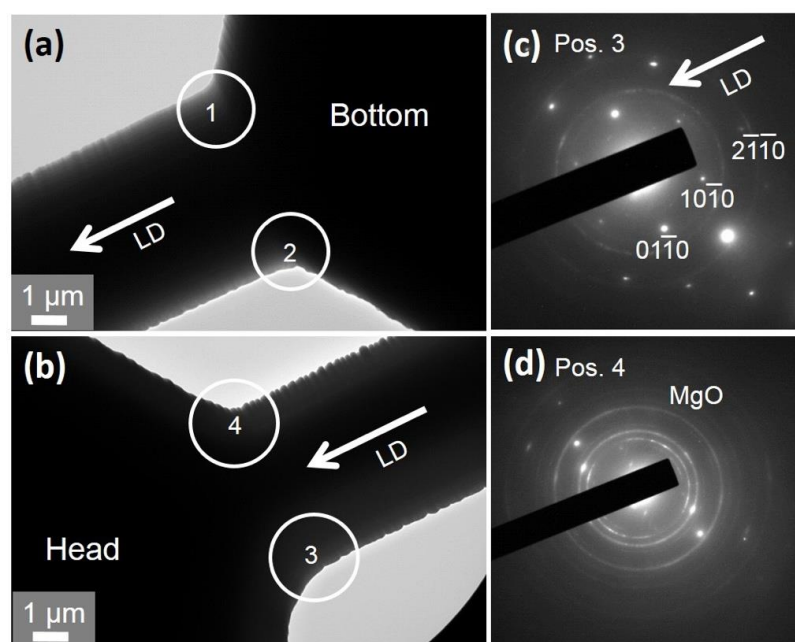

Figure 3. Pre-testing TEM analysis of a 4 μm thick Mg tensile sample, showing the gauge section towards the bottom (**a**) and head part (**b**), respectively. The diffraction patterns in (**c**) show the expected crystallography, while the image in (**d**) indicates redeposition of a nanocrystalline MgO layer. A white arrow indicates loading direction in real and reciprocal space.

To cover a number of possible deformation mechanisms [30], we examined loading directions along $Mg[2\bar{1}\bar{1}2]$, $Mg[0001]$, and $Mg[2\bar{1}\bar{1}0]$, respectively. An overview of the respective orientations, loading modes (compression/tension) and the Schmid factors corresponding on the one hand to dislocation plasticity on the basal, prismatic or pyramidal plane, and on the other hand to tension or contraction twinning, respectively, are given in Table 1. In addition, the deformation mode noted in the in-situ experiments as detailed later is noted. To relate this crystal orientation information to the testing geometry, in

Figure 4 the different crystal orientations are visualised in combination with the unit cell and the expected deformation mechanisms based on the actual Schmid [30].
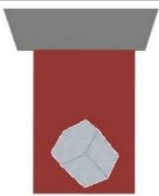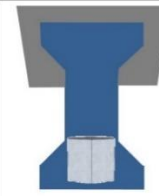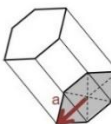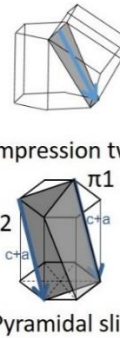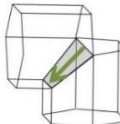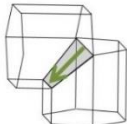

Figure 4. Schematic overview of the studied crystal orientations, the related unit cell orientation with respect to the uniaxial testing volume, and the conceivable deformation mechanism(s). The introduced colour code is kept consistent throughout the manuscript.

To load the compression samples, a conical conductive diamond tip with a 16-μm diameter flat punch (Synton MDP, Nidau, Switzerland) was used, while for tensile testing, a gripping tool FIB fabricated from a heavily drawn W wire was employed [23]. Before running the actual deformation experiments, the stiffness of the respective lamella was determined for later compliance corrections. The miniaturised in-situ compression and tensile tests were conducted under displacement control at a nominally constant strain rate of $1 \cdot 10^{-3}$ s^{-1}, and a corresponding video of the experiment was recorded using a frame grabber at a repetition rate of 1 Hz. This allows for a trade-off between temporal resolution upon direct observation and sufficient signal-to-noise ratio for later digital image analysis, pillar sink-in correction, and analysis of local strain, respectively.

Table 1. Summary of Mg crystal orientations tested, loading mode, nominal Schmid factors, and experimentally observed deformation mode.

Loading Direction	Loading Mode	Schmid Factor for Feformation by						Observed Deformation Mode
[-]	[-]	\<a\> Basal Slip	\<a\> Prismatic Slip	\<c+a\> Pyramidal (π1) Slip	\<c+a\> Pyramidal (π2) Slip	Tension Twinning	Contraction Twinning	
Mg $[2\bar{1}\bar{1}2]$	Compression	0.5	0.2	0.39	0.30	-	0.32	Basal slip
Mg $[0001]$	Compression	0	0	0.4	0.45	-	0.42	Pyramidal slip
Mg $[0001]$	Tension	0	0	0.4	0.45	0.5	-	Tensile twin
Mg $[2\bar{1}\bar{1}0]$	Compression	0	0.43	0.4	0.45	0.37	-	Tensile twin and basal slip in the twin

3. Results and Discussion

Considering the TEM analysis in Figure 3a,b, it is possible to note that the specimen corner is not as sharp and smooth as one might expect. This results from the very high sputtering rates of Mg in conjunction with the broadening of the ion beam. Moreover, we note that the roughness is more pronounced along the upper sides, related to diffraction analysis spots one and four, respectively. From the indicated loading direction and the electron diffraction information in Figure 3c, it is evident that the sample is loaded along the intended $[2\bar{1}\bar{1}0]$ direction. While there is slight indication of additional diffraction rings in this image, they are much more pronounced in Figure 3d and can be indexed as MgO. Thus, we consider that the bottom side of the tensile sample was polished last during FIB preparation. As such, there is a rather smooth edge and only a minimal amount of nanocrystalline MgO on the surface. Contrarily, on the upper side that was finished before, redeposition of sputtered Mg could take place, causing a rougher surface that is more prone to oxidation, thereby explaining the rougher appearance and more distinct MgO diffraction signal. Thus, we conclude that we can assure that the crystal orientation for our samples is uniform and consistent with expectations, but there is a nanocrystalline MgO layer that could affect the observability of surface features during in-situ SEM testing and might in the worst case act as a confining hard shell. Mg is known to form an oxide easily, and we observed such an MgO layer previously, in particular upon heat treatments of nanoscale Mg pillars [31]. However, for the given situation of few micrometre sized pillars and few nm thick oxide layer, we do not expect pronounced influences in terms of a confining layer.

We start with the deformation mode easiest to activate in Mg, basal slip. As evident for the 4-μm sized Mg$[2\bar{1}\bar{1}2]$ micro-compression specimen shown in Figure 5, the flow curve in Figure 5a exhibits some minor and one major event during plastic deformation, which takes place at flow stresses in the range of 60–80 MPa. These events can be directly correlated to slip steps emerging on the sample surface during testing, as shown in the inset to Figure 5a. This is further supported by inclined post-mortem SEM images taken from the front and back, where one large and one smaller slip step are well discerned (Figure 5c,d). This localised slip behaviour was also reported earlier [12] and is in excellent agreement to common observations for dislocation slip based on a limited number of dislocation sources in other metals exhibiting a low Peierls barrier [23]. Given the sample crystallography and observed slip plane inclination, it is certain to ascribe this plastic deformation to basal slip [12]. A feature of note here is the oxide layer well displayed on the detail of an approximately 400 nm wide mayor slip step (Figure 5b). This MgO layer has a thickness of ~10 nm [31] and stretches conformal over the emerged slip step, which required roughly 1200 basal plane dislocations with $[11\bar{2}0]$ direction to exit in order to form the slip step. The important implication is that this MgO layer does not break easily and thus has the tendency to cover faint surface steps. Thus, it cannot be determined with certainty whether the other smaller features along the stress–strain curve correspond to reactivation of dislocation sources that already operated and produced a multitude of dislocations resulting in observable slip steps, or the activation of new sources with resultant slip steps that might be not well discernible on the specimen surface yet due to this oxide layer. However, considering that it is considerably harder to nucleate dislocations from an interface than to mobilise pre-existing ones, it seems likely that some residual defects allowed for generation of a dislocation source (classically Frank–Read type, double cross-slip type or single armed source type) in the interior of the specimens.
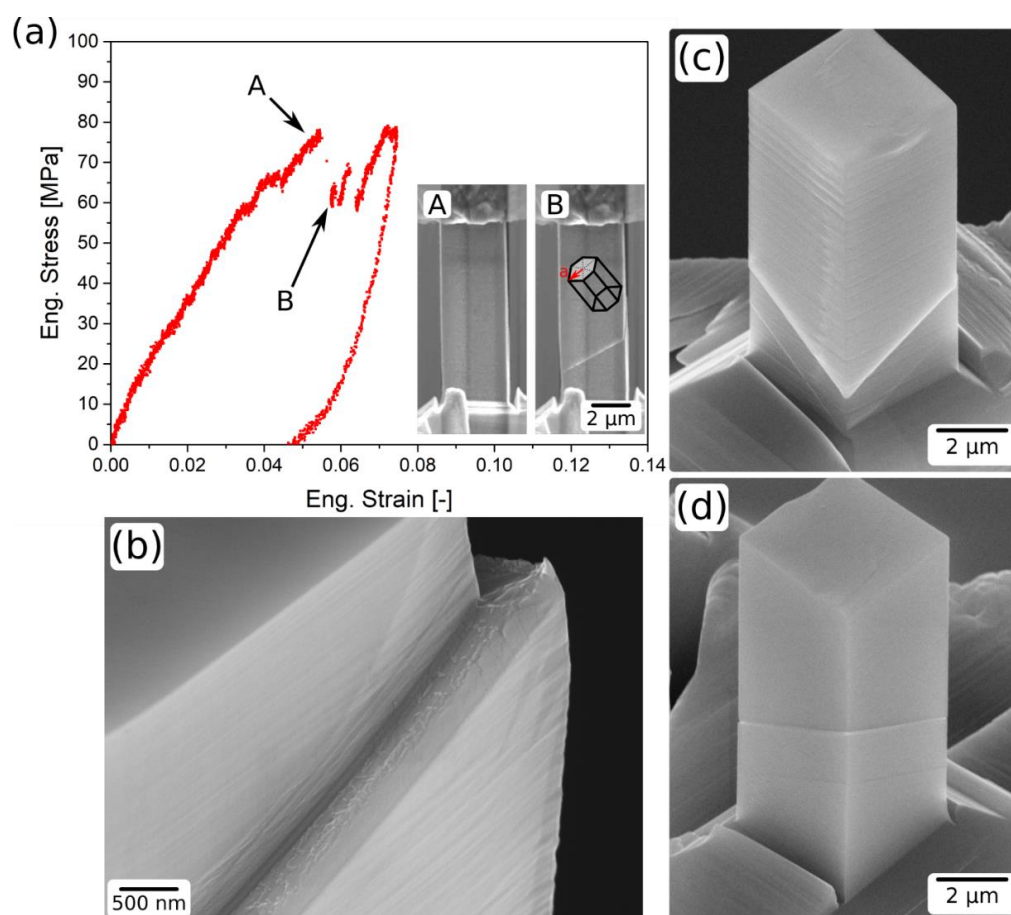
Figure 5. Micro-compression test on a 4-μm Mg$[2\bar{1}\bar{1}2]$ pillar. (**a**) Stress–strain behaviour showing some minor plastic events and one mayor stress drop. The inset depicts still images of the sample at points A and B of the experiment, as well as the crystal unit cell. (**b**) Detailed post mortem inspection of a large slip offset. (**c,d**) Front and backside view of the sample after testing, indicating a large and a smaller surface steps on the specimen surface.

Turning to the 4-μm Mg[0001]-oriented sample shown in Figure 6, we note that the stress–strain data in Figure 6a exhibit an initial linear elastic regime followed by a yield point at ~275 MPa, to be continued by a plastic deformation period exhibiting pronounced strain hardening. The loading portion of the curve exhibits a noticeable bend indicative of slight misalignment between sample and flat punch, while the deduced elastic modulus amounts to ~40 GPa, which is in reasonable accordance with calculated orientation dependent values [32] based on experimental elastic constants [33] and lattice spacing [34] as summarised in Table 2. Since local plastic deformation should correct for the local contact issues at the initial loading, the lower experimental value upon elastic unloading from a plastically deformed sample might result from a non-perfect accounting of parasitic compliance effects, which could be eliminated, for example, by measuring the deformation directly on the sample surface using digital image correlation [35]. Alternatively, this could originate from the reverse motion and straightening of bulged out dislocations upon unloading, similar to what is frequently referred to as a Bauschinger effect in bending geometries [36]. In that case in-situ TEM observations could help to clarify the origin, but this goes beyond the scope of this work. The images recorded during in-situ deformation as well as after loading (Figure 6b) display a distinct shortening of the sample, but only minimal traces of deformation on the surface, in fact the most pronounced notion is a certain sample barrelling. Loading along this crystal direction should suppress basal and prismatic slip, as well as $\{10\bar{1}2\}$ twinning. Still, macroscopic compression tests on Mg[0001] reported a certain amount of twinning to take place due to barrelling and

friction effects [37]. Turning to the present miniaturised compression test, we note only a slight discontinuity at a stress of ~275 MPa, but the absence of a flow plateau that could be indicative of a limited propagation of a $\{10\bar{1}1\}$ compression twin. This is not too surprising, as during compression twinning the twinned part would have to rotate significantly out of the loading axis (Figure 4), which is constrained by the laterally stiff sample setup and the friction between specimen and diamond flat punch [38]. However, a significant amount of work hardening is displayed, which favourably corresponds to the activation of pyramidal slip. As post mortem EBSD investigation further confirmed the absence of twinning, this discrete burst is explained by the avalanche-like activation of pyramidal slip on various planes, leading to the increased dislocation density and resultant work hardening in these microscale specimens. In general, it should be recognised that the formation and growth of a compression twin during compressive loading (see Figure 4) would yield a favourable configuration for subsequent basal slip, which is not observed and therefore further validates the assumption that the majority of deformation is carried by dislocation plasticity on pyramidal (π1 or π2) slip planes.
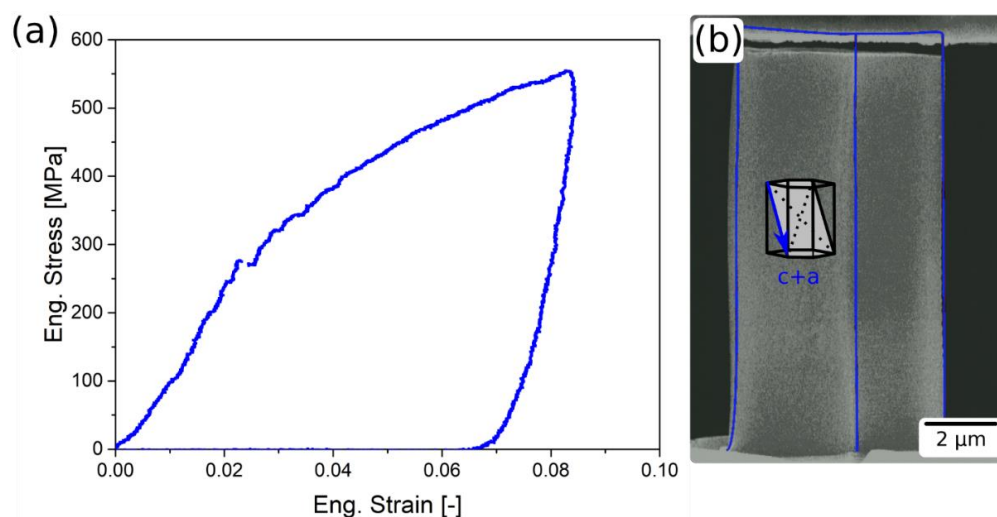

Figure 6. Micro-compression test on a 4-μm Mg[0001] specimen. (**a**) Stress-strain characteristic and (**b**) deformed specimen. Blue lines indicate original specimen geometry, while the inset indicates the unit cell and slip crystallography.

Table 2. Orientation dependent Young's moduli and Poisson's ratios for the cylindrically symmetrical Mg single crystal.

Crystal Orientation	Young's Moduls E (GPa)	Poisson's Ratio v (-)
$< 0001 >$	48.3	0.214
$< 10\bar{1}0 >$, $< 11\bar{2}0 >$	46.2	0.343

Relating this behaviour to the previously shown $\left[2\bar{1}\bar{1}2\right]$ specimen, the strains at the first deviation from linear elasticity are similar, but the stress is about a factor of four higher in the [0001] specimen, which is expected in light of the different mechanisms (pyramidal slip versus basal slip). The fact that there are no pronounced slip bands is in accordance with the argument that deformation is mostly driven by pyramidal slip, as the higher number of available slip planes can lead to dislocation interaction and formation of kinks or jogs. Moreover, due to the large Burgers vector of <c+a> dislocations, they are dissociated into two partial dislocations. A recent study showed that those are intrinsically transformed to basal-dissociated immobile dislocation structures, which cannot contribute to plastic deformation, but serve as strong obstacles to the motion of all other dislocations inside the pillar [14], resulting in the strong strain hardening observed in the [0001] specimen. This is clearly different to the $\left[2\bar{1}\bar{1}2\right]$ specimen, where the predominant deformation occurs on the

basal plane, having only two independent slip systems. Furthermore, the lack of "strain-burst" type behavior in conjunction with the high strain hardening suggest no or only a minor occurrence of twinning, as previously shown macroscopically by Syed et al. [37].

To underline the previous point regarding difficult to activate deformation mechanisms and deformation constraints, we consider another miniaturised compression test on a Mg[1000] specimen with 2 μm width in Figure 7. Similar to the previous example, the stress-strain data shown in Figure 7a does not exhibit a distinct yield event, but a gradual elastic–plastic transition. At a stress of ~185 MPa a flow plateau is observed, corresponding to a distortion of the micro-compression sample evident in Figure 7c. After the distinct load-drop at a strain of 0.07, we observe the emergence of a distinct slip step at the position of the previous specimen distortion (Figure 7d), which grows during deformation at a constant flow stress of about 160 MPa. While the initial unloading slope appears quite similar to that upon initial loading, the unloading curve develops a remarkable bend back, indicative of a significant amount of reverse plasticity. Alternatively, this could be ascribed to geometric changes occurring during the experiment. We attribute the gradual elastic–plastic transition again to pyramidal slip activity, and the constant flow plateau to the activation of basal slip in the locally modified crystallography of the deformed specimen. Initially, this basal slip is confined by the surface oxide layer. Once this breaks at the distinct stress drop, the slip step becomes well discernible on the sample surface and grows with continuing deformation.

Coming back to the previously mentioned aspect of confinement effects on twinning, we conducted related micro-tensile tests on an Mg[0001] crystal orientation using a 4-μm tensile sample in Figure 8, as this would permit the formation of a tension twin. As reported earlier, the longer aspect ratio tensile geometry is more compliant and allows for lateral adjustments [38]. In Figure 8a, we observe an elastic–plastic transition followed by a rather constant flow stress in the range of 80 to 90 MPa. This corresponds well to the nucleation and growth of a tensile twin seen in in Figure 8d,e. The pronounced load drop at a strain of 0.08 relates to the nucleation of a second tensile twin on the left hand side of the tensile specimen, as also indicated in the in-situ image shown as Figure 8f. Taking the specimen back into the TEM after unloading, in Figure 8b we observe the distinct crystal orientation change at the twin front in the area indicated by a dashed rectangle in Figure 8f. Thus, this setup allows for the unhindered nucleation and propagation of tensile twins.
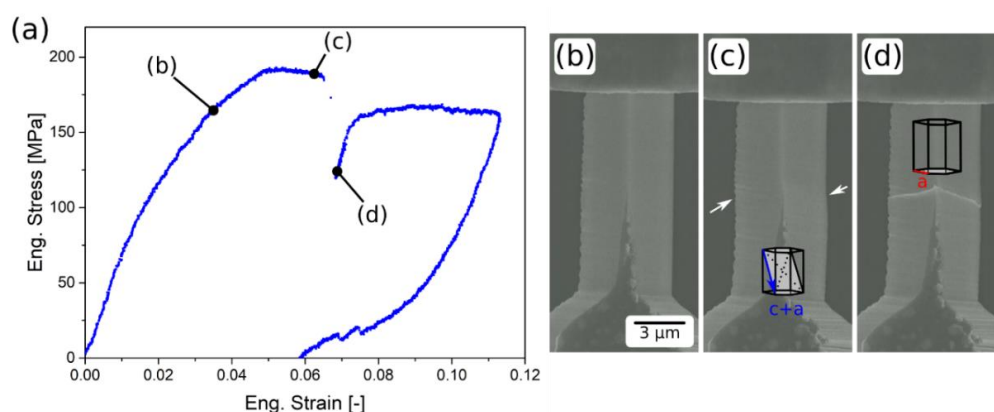

Figure 7. Micro-compression testing on a 2-μm Mg[0001] sample. (**a**) Stress-strain curve showing an extended elastic–plastic transition, followed by a distinct load drop and a flow plateau. Notably, the unloading portion exhibits a remarkable amount of reverse plasticity. (**b–d**) In-situ images in correlation to the flow curve, documenting the onset of plasticity by pyramidal slip, the nucleation of basal slip and the continuous growth of the related almost horizontal slip step.
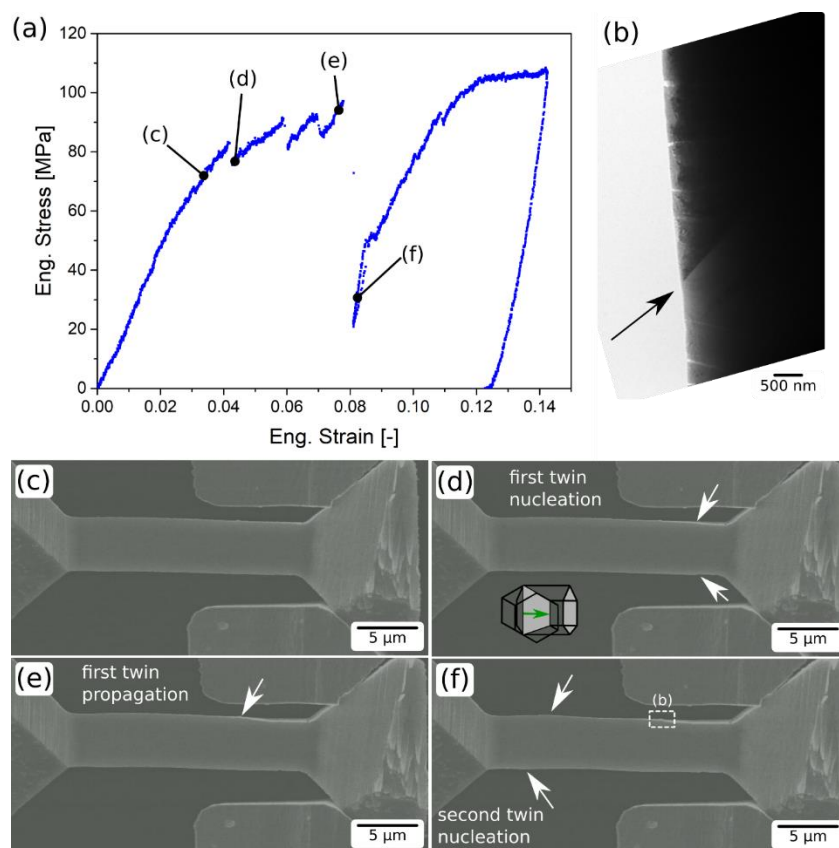
Figure 8. Micro-tensile test of a 4-μm Mg[0001] sample. (**a**) Stress–strain curve and (**b**) post mortem TEM image showing the formed twin boundary indicated by an arrow. (**c**–**f**) In-situ SEM images as indicated in (**a**), corresponding to the yield point, initiation of the first tensile twin, propagation of the twin, and nucleation of a second twin, respectively. The area inspected by TEM in (**b**) is indicated in (**f**).

It is well known that Mg exhibits two distinctly different twins when compressed ($\{10\bar{1}1\}$ contraction twin) or elongated ($\{10\bar{1}2\}$ tensile twin) along the [0001] axis. While the so called contraction twin is only rarely observed because of the higher activation threshold, tensile twinning is observed frequently and considered a major carrier of deformation in Mg. The slight twist in the tensile specimen might have worked as a catalyst for twin nucleation, but it is definitely the more favourable loading direction for tensile twinning. After first and second twinning events occur, the loading axis of the pillar is changed from [0001] to ~$[10\bar{1}0]$ because the crystal is reoriented by 86° upon twinning. Under $[10\bar{1}0]$ tensile loading, the contraction twin would be crystallographically favoured, but the critical resolved shear stress for contraction twinning is much higher than 90 MPa. This makes activation of another twin within the twinned part very unlikely.

An interesting notion is that the threshold for twinning does not seem to be constant. Previously, we showed that the nucleation of deformation twins is not a purely stress driven process, but is triggered by dislocation bulges on the prismatic plane [39], which are dependent on the very local stress and strain state and can therefore not always be derived just from considering a global stress value.

To compare the tensile twinning observed in tension to the activation of the same mechanism in compression, the last example concerns a miniaturised compression test of a 2-μm wide specimen along the Mg$[2\bar{1}\bar{1}0]$ direction. For this crystallographic orientation, due to the specific crystal rotation created by the twin, lateral confinement effects should be less pronounced and thus also allow twinning to take place during compression. In fact, this specific orientation was previously studied by our group in a combined in-situ SEM and in-situ TEM fashion and we will therefore be rather brief and only mention the

essential facts, while all details can be found elsewhere [39]. In Figure 9a, we again observe a clear elastic regime followed by a distinct burst and load drop at a stress of about 400 MPa, followed by an overshoot of the indenter due to a not sufficiently fast feedback control, thereby releasing the strain energy stored in the system. Distinct distortion of the specimen geometry, in fact a slight kink of the top part due to the twinning reorientation by 86°, is seen in point B in the inset upon elastic reloading. Thus, we can assign this again to the nucleation and propagation of a tensile twin. After elastic reloading, we observe a constant stress plateau at ~200 MPa, where slip steps emerge as seen in the inset corresponding to point C along the stress–strain data. This corresponds to basal slip in the twinned part of the specimen, as reported earlier [39]. In Figure 9b an inclined post mortem SEM image shows the slip steps in more detail.
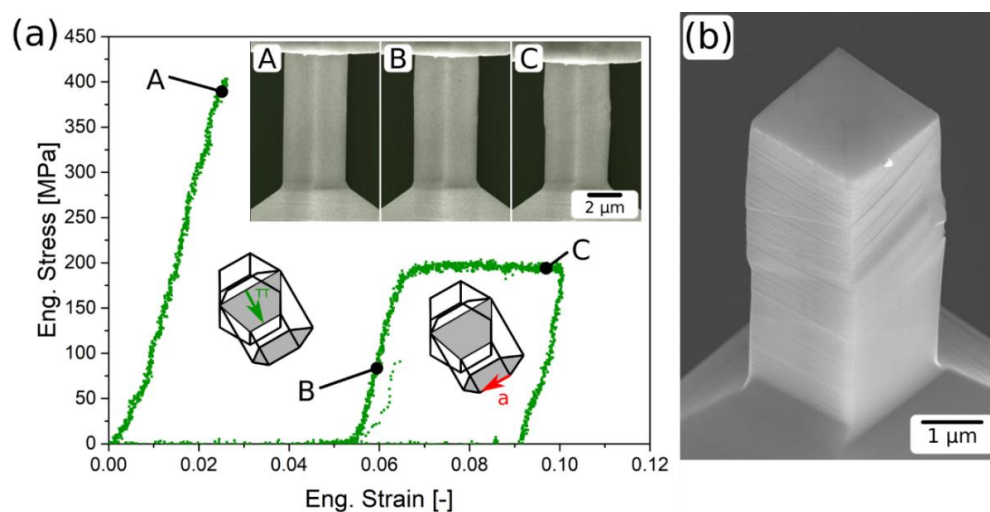

Figure 9. In-situ SEM micro-compression test of a 2-µm Mg $[2\overline{1}\overline{1}0]$ sample. (**a**) Stress–strain data showing elastic limit, a distinct plastic event followed by reloading, a plateau stress, and final unloading. Corresponding still images from the in-situ video relating to points A–C indicated in the stress–strain curve are provided as insets. (**b**) Inclined post mortem image of the deformed specimen, showing a slight tilt of the twinned part, as well as slip steps within this sample portion.

It is noteworthy that for the smaller 2-µm specimen examined here, the flow stress for basal slip is in the range of 200 MPa, while we measured only about 70 MPa for the 4-µm sample in Figure 5. This is mostly due to the sample size effect, with additional contributions from different Schmid factors to be accounted for.

To depict all discussed specimens in a comparative framework, the different critical resolved shear stresses (CRSS) were calculated, based on the Schmid factors summarised in Table 1, and are shown with respect to the different observed deformation mechanisms in Figure 10. There, the full symbols correspond to the first evident deviation from linear elastic loading as an indication for the beginning of the respective yield phenomena, while the open symbols correspond to the subsequent evident features of deformation: load drop corresponding to the large slip step for the $[2\overline{1}\overline{1}2]$ specimen, load drop corresponding to the second evident twin formation for the [0001] tension specimen, and basal slip plateau following twinning for the $[2\overline{1}\overline{1}0]$ specimen, respectively. The initial pyramidal slip CRSS occurring in the [0001] compression specimen was calculated for both, π1 and π2 slip, as the exact configuration is not known. However, based on the fact that π1 slip results in a lower CRSS, it can be assumed that it is easier to activate and therefore the majority contribution to plasticity in this specimen. This would also be in agreement with current observations by Xie et al. [40].
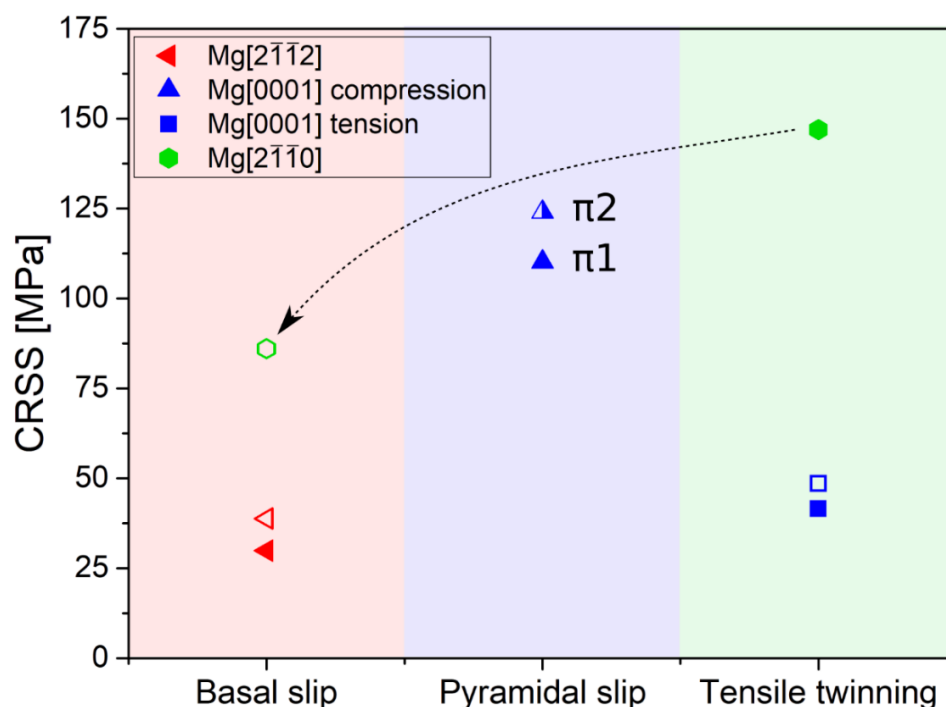
Figure 10. Critical resolved shear stresses (CRSS) of the previously detailed samples with regard to deformation mechanisms. The filled symbols represent initial deviation of the elastic load-displacement regime, while the open symbols depict evident deformation features, such as large load drops, which correspond to the respective mechanisms. For the Mg[0001] compression specimen, CRSS was calculated for both pyramidal planes (π1, π2) for comparison.

Comparing now the CRSS for tensile twinning in tension and compression as provided in Figure 10, it is evident that the necessary nucleation stress is considerably higher (~250%) for the 2-μm compression configuration than for the 4-μm tensile configuration. This could be partially attributed to the smaller geometric dimensions but seems unlikely to be a satisfying single cause explanation for this pronounced difference. Considering, however, not resolved stress but strain one could argue that the tensile strain along the [0001] direction is $\varepsilon_{tensile} = \frac{\sigma}{E_{<0001>}} = 0.00173$ in the tensile specimen, while it is $\varepsilon_{compression} = \frac{\sigma}{E_{<11\bar{2}0>}}\nu_{<11\bar{2}0>} = 0.00298$ for the compression specimen, which is only an increase of ~60% for a sample size reduction by a factor of 2. Furthermore, this train of thought suggests that tensile twinning in Mg is rather a strain driven than a stress driven process.

In comparison with literature values concerning CRSS as summarised by Zhang and Joshi [30], our values are a factor 5–10 higher for basal slip and tensile twinning, and about a factor 2–3 higher for pyramidal slip. This could, even though not desired in the first place, again be related to be resultant of the small size of the samples. However, specifically in basal slip configuration with typical CRSS values in the single digit MPa range, it could also be a result of the high lateral stiffness in compression testing which causes a constrained deformation field [41], or additional pile-up contributions from FIB damage [42,43] or the thin MgO layer [31].

As evident from the previously shown experiments, the remarkable difference between easy and hard deformation modes in anisotropic materials such as Mg renders it rather challenging to probe specific mechanisms individually. However, as shown in the examples given above, it is well feasible, in particular when complemented by in-situ observations or respective post characterisation. In contrast, for a bulk experiment on a polycrystalline sample such differentiations would not be possible, as local stresses would always cause the unwanted activation of easy deformation mechanisms such as basal slip, either long before the actual hard mode is activated, or right after the crystal lattice was changed to a favourable orientation by local lattice distortions or twinning.

In terms of detailed insights and concrete dislocation or twinning mechanisms, a combined in-situ SEM/TEM study might be preferred, as the larger SEM experiments deliver bulk quantities if conducted on large enough specimens [28,44], while the TEM observations identify specific dislocation character or twinning relationships [39]. It should, however, be kept in mind that the different mechanisms could exhibit various strength scaling characteristics [10,18]. As such, for small enough specimens a transition between plastic mechanisms could occur [44] and mislead the data interpretation. Even changes in dislocation dynamics due to the high stresses in such highly confined nanoscale volumes are conceivable [45]. Therefore, such an undertaking ideally encompasses a complete size-dependent assessment.

From the more general application perspective, in our present work we turned to extraction of differently oriented lamellas from a bulk piece of single crystalline material. For experimental polycrystalline materials or alloys, this can easily be further reduced with respect to required material, say down to a specific single grain. Therefore, the extraction of lift-out lamellas from the grain of interest under specific orientations with respect to the surface normal, or from different grains with suited orientations, in a pick and place operation using a micromanipulator would be a feasible way [46]. As this most certainly requires larger amounts of surrounding material to be removed, modern developments such as Xe-FIBs or femtosecond laser machining [47,48] might prove helpful. Alternatively, different sample holders could be 3D printed to tilt the grain to the different selected orientations [7]. The only challenge remaining in that case is to FIB machine the sample top surface perpendicular with respect to the loading axis of the specimen situated within the tilted sample surface, as this requires a 90° tilting of the mounted sample.

4. Conclusions

In the present work, on the example of the hexagonal metal Mg, we attempted a depictive overview to highlight that markedly different deformation mechanisms in anisotropic materials can be quantitatively examined. To do so, it is instructive to choose suited crystallographic orientations for the small scale testing from the bulk of interest, and to avoid mechanical constraints that could promote activation of unintended deformation mechanisms. Furthermore, the crystal reorientation due to twinning and related changes in the preferably activated deformation mechanisms should be kept in mind. Finally, while the mechanical signature and post mortem observations should suffice for analysing the respective deformation mechanisms, direct in-situ observation lends itself to simplify this process significantly and provide better insight into the dynamics and temporal sequence.

Conflicts of Interest: The authors declare no conflict of interest.

References

1. Uchic, M.D.; Dimiduk, D.M.; Florando, J.N.; Nix, W.D. Sample dimensions influence strength and crystal plasticity. *Science* **2004**, *305*, 986–989. [CrossRef] [PubMed]
2. Uchic, M.D.; Shade, P.A.; Dimiduk, D. Plasticity of micrometer-scale single crystals in compression. *Ann. Rev. Mater. Res.* **2009**, *39*, 361–386. [CrossRef]

3. Greer, J.R.; de Hosson, J.T.M. Plasticity in small-sized metallic systems: Intrinsic versus extrinsic size effect. *Prog. Mater. Sci.* **2011**, *56*, 654–724. [CrossRef]

4. Malyar, N.V.; Micha, J.S.; Dehm, G.; Kirchlechner, C. Size effect in bi-crystalline micropillars with a penetrable high angle grain boundary. *Acta Mater.* **2017**, *129*, 312–320. [CrossRef]

5. Fritz, R.; Maier-Kiener, V.; Lutz, D.; Kiener, D. Interplay between sample size and grain size: Single crystalline vs. ultrafine-grained chromium micropillars. *Mater. Sci. Eng. A* **2016**, *674*, 626–633. [CrossRef]

6. Kheradmand, N.; Vehoff, H. Orientation Gradients at Boundaries in Micron-Sized Bicrystals. *Adv. Eng. Mater.* **2012**, *14*, 153–161. [CrossRef]

7. Liebig, J.P.; Krauß, S.; Göken, M.; Merle, B. Influence of stacking fault energy and dislocation character on slip transfer at coherent twin boundaries studied by micropillar compression. *Acta Mater.* **2018**, *154*, 261–272. [CrossRef]

8. Byer, C.M.; Li, B.; Cao, B.; Ramesh, K.T. Microcompression of single-crystal magnesium. *Scr. Mater.* **2010**, *62*, 536–539. [CrossRef]

9. Lilleodden, E. Microcompression study of Mg (0 0 0 1) single crystal. *Scr. Mater.* **2010**, *62*, 532–535. [CrossRef]

10. Yu, Q.; Shan, Z.-W.; Li, J.; Huang, X.; Xiao, L.; Sun, J.; Ma, E. Strong crystal size effect on deformation twinning. *Nature* **2010**, *463*, 335–338. [CrossRef]

11. Guo, Y.; Schwiedrzik, J.; Michler, J.; Maeder, X. On the nucleation and growth of {112$\bar{}$2} twin in commercial purity titanium: In situ investigation of the local stress field and dislocation density distribution. *Acta Mater.* **2016**, *120*, 292–301. [CrossRef]

12. Ye, J.; Mishra, R.K.; Sachdev, A.K.; Minor, A.M. In situ TEM compression testing of Mg and Mg—0.2 wt.% Ce single crystals. *Scr. Mater.* **2011**, *64*, 292–295. [CrossRef]

13. Wu, Z.; Ahmad, R.; Yin, B.; Sandlöbes, S.; Curtin, W.A. Mechanistic origin and prediction of enhanced ductility in magnesium alloys. *Science* **2018**, *359*, 447–452. [CrossRef] [PubMed]

14. Wu, Z.; Curtin, W.A. The origins of high hardening and low ductility in magnesium. *Nature* **2015**, *526*, 62–67. [CrossRef] [PubMed]

15. Liu, B.-Y.; Liu, F.; Yang, N.; Zhai, X.-B.; Zhang, L.; Yang, Y.; Li, B.; Li, J.; Ma, E.; Nie, J.-F.; et al. Large plasticity in magnesium mediated by pyramidal dislocations. *Science* **2019**, *365*, 73–75. [CrossRef]

16. Li, B.; Ma, E. Atomic shuffling dominated mechanism for deformation twinning in magnesium. *Phys. Rev. Lett.* **2009**, *103*, 035503. [CrossRef]

17. Ostapovets, A.; Molnár, P. On the relationship between the "shuffling-dominated" and "shear-dominated" mechanisms for twinning in magnesium. *Scr. Mater.* **2013**, *69*, 287–290. [CrossRef]

18. Liu, Y.; Li, N.; Kumar, M.A.; Pathak, S.; Wang, J.; McCabe, R.J.; Mara, N.A.; Tomé, C.N. Experimentally quantifying critical stresses associated with basal slip and twinning in magnesium using micropillars. *Acta Mater.* **2017**, *135*, 411–421. [CrossRef]

19. Prasad, K.E.; Rajesh, K.; Ramamurty, U. Micropillar and macropillar compression responses of magnesium single crystals oriented for single slip or extension twinning. *Acta Mater.* **2014**, *65*, 316–325. [CrossRef]

20. Wang, J.; Molina-Aldareguía, J.M.; Llorca, J. Effect of Al content on the critical resolved shear stress for twin nucleation and growth in Mg alloys. *Acta Mater.* **2020**, *188*, 215–227. [CrossRef]

21. Wang, J.; Ramajayam, M.; Charrault, E.; Stanford, N. Quantification of precipitate hardening of twin nucleation and growth in Mg and Mg-5Zn using micro-pillar compression. *Acta Mater.* **2019**, *163*, 68–77. [CrossRef]

22. Zhang, H.; Schuster, B.E.; Wei, Q.; Ramesh, K.T. The design of accurate micro-compression experiments. *Scr. Mater.* **2006**, *54*, 181–186. [CrossRef]

23. Kiener, D.; Grosinger, W.; Dehm, G.; Pippan, R. A further step towards an understanding of size-dependent crystal plasticity: In-situ tension experiments of miniaturized single crystal copper samples. *Acta Mater.* **2008**, *56*, 580–592. [CrossRef]

24. Moser, G.; Felber, H.; Rashkova, B.; Imrich, P.J.; Kirchlechner, C.; Grosinger, W.; Motz, C.; Dehm, G.; Kiener, D. Sample Preparation by Metallography and Focused Ion Beam for Nanomechanical Testing. *Pract. Metallogr.* **2012**, *49*, 343–355. [CrossRef]

25. Wurster, S.; Treml, R.; Fritz, R.; Kapp, M.W.; Langs, E.; Alfreider, M.; Ruhs, C.; Imrich, P.J.; Felber, G.; Kiener, D. Novel Methods for the Site Specific Preparation of Micromechanical Structures. *Pract. Metallogr.* **2015**, *52*, 131–146. [CrossRef]

26. Kiener, D.; Zhang, Z.; Sturm, S.; Cazottes, S.; Imrich, P.J.; Kirchlechner, C.; Dehm, G. Advanced nanomechanics in the TEM: Effects of thermal annealing on FIB prepared Cu samples. *Philos. Mag. A* **2012**, *92*, 3269–3289. [CrossRef]

27. Schneider, A.S.; Kiener, D.; Yakacki, C.M.; Maier, H.J.; Gruber, P.A.; Tamura, N.; Kunz, M.; Minor, A.M.; Frick, C.P. Influence of bulk pre-straining on the size effect in nickel compression pillars. *Mater. Sci. Eng. A* **2013**, *559*, 147–158. [CrossRef]

28. El-Awady, J.A. Unravelling the physics of size-dependent dislocation-mediated plasticity. *Nat. Commun.* **2015**, *6*, 5926. [CrossRef]

29. Maass, R.; van Petegem, S.; Grolimund, D.; van Swygenhoven, H.; Uchic, M.D. A strong micropillar containing a low angle grain boundary. *Appl. Phys. Lett.* **2007**, *91*, 131909. [CrossRef]

30. Zhang, J.; Joshi, S.P. Phenomenological crystal plasticity modeling and detailed micromechanical investigations of pure magnesium. *J. Mech. Phys. Solids* **2012**, *60*, 945–972. [CrossRef]

31. Jeong, J.; Lee, S.; Kim, Y.; Han, S.M.; Kiener, D.; Kang, Y.-B.; Oh, S.H. Microstructural evolution of a focused ion beam fabricated Mg nanopillar at high temperatures: Defect annihilation and sublimation. *Scr. Mater.* **2014**, *86*, 44–47. [CrossRef]

32. Zhang, J.-M.; Zhang, Y.; Xu, K.-W.; Ji, V. Anisotropic elasticity in hexagonal crystals. *Thin Solid Films* **2007**, *515*, 7020–7024. [CrossRef]

33. Slutsky, L.J.; Garland, C.W. Elastic Constants of Magnesium from 4.2 K to 300 K. *Phys. Rev.* **1957**, *107*, 972–976. [CrossRef]

34. Von Batchelder, F.W.; Raeuchle, R.F. Lattice Constants and Brillouin Zone Overlap in Dilute Magnesium Alloys. *Phys. Rev.* **1957**, *105*, 59–61. [CrossRef]

35. Moser, B.; Wasmer, K.; Barbieri, L.; Michler, J. Strength and fracture of Si micropillars: A new scanning electron microscopy-based micro-compression test. *J. Mater. Res.* **2007**, *22*, 1004–1011. [CrossRef]

36. Kapp, M.W.; Kirchlechner, C.; Pippan, R.; Dehm, G. Importance of dislocation pile-ups on the mechanical properties and the Bauschinger effect in microcantilevers. *J. Mater. Res.* **2015**, *30*, 791–797. [CrossRef]

37. Syed, B.; Geng, J.; Mishra, R.K.; Kumar, K.S. Compression response at room temperature of single-crystal magnesium. *Scr. Mater.* **2012**, *67*, 700–703. [CrossRef]

38. Kiener, D.; Grosinger, W.; Dehm, G. On the importance of sample compliance in uniaxial microtesting. *Scr. Mater.* **2009**, *60*, 148–151. [CrossRef]

39. Jeong, J.; Alfreider, M.; Konetschnik, R.; Kiener, D.; Oh, S.H. In-situ TEM observation of twin-dominated deformation of Mg pillars: Twinning mechanism, size effects and rate dependency. *Acta Mater.* **2018**, *158*, 407–421. [CrossRef]

40. Xie, K.Y.; Alam, Z.; Caffee, A.; Hemker, K.J. Pyramidal I slip in c-axis compressed Mg single crystals. *Scr. Mater.* **2016**, *112*, 75–78. [CrossRef]

41. Kiener, D.; Motz, C.; Dehm, G. Micro-compression testing: A critical discussion of experimental constraints. *Mater. Sci. Eng. A* **2009**, *505*, 79–87. [CrossRef]

42. Kiener, D.; Motz, C.; Rester, M.; Dehm, G. FIB damage of Cu and possible consequences for miniaturized mechanical tests. *Mater. Sci. Eng. A* **2007**, *459*, 262–272. [CrossRef]

43. Hütsch, J.; Lilleodden, E.T. The influence of focused-ion beam preparation technique on microcompression investigations: Lathe vs. annular milling. *Scr. Mater.* **2014**, *77*, 49–51. [CrossRef]

44. Kiener, D.; Hosemann, P.; Maloy, S.A.; Minor, A.M. In situ nanocompression testing of irradiated copper. *Nat. Mater.* **2011**, *10*, 608–613. [PubMed]

45. Wang, J.W.; Zeng, Z.; Weinberger, C.R.; Zhang, Z.; Zhu, T.; Mao, S.X. In situ atomic-scale observation of twinning-dominated deformation in nanoscale body-centred cubic tungsten. *Nat. Mater.* **2015**, *14*, 594–600. [PubMed]

46. Hirakata, H.; Takahashi, Y.; Truong, D.; Kitamura, T. Role of plasticity on interface crack initiation from a free edge and propagation in a nano-component. *Int. J. Fract.* **2007**, *145*, 261–271.

47. Echlin, M.P.; Mottura, A.; Torbet, C.J.; Pollock, T.M. A new TriBeam system for three-dimensional multimodal materials analysis. *Rev. Sci. Instrum.* **2017**, *83*, 023701. [CrossRef]

48. Pfeifenberger, M.J.; Mangang, M.; Wurster, S.; Reiser, J.; Hohenwarter, A.; Pfleging, W.; Kiener, D.; Pippan, R. The use of femtosecond laser ablation as a novel tool for rapid micro-mechanical sample preparation. *Mater. Des.* **2017**, *121*, 109–118. [CrossRef]